

## Retraction

# Retracted: Study on the 2D Optimization Simulation of Complex Five-Hole Cutting Blasting under Different Lateral Pressure Coefficients

### Complexity

Received 23 January 2024; Accepted 23 January 2024; Published 24 January 2024

Copyright © 2024 Complexity. This is an open access article distributed under the Creative Commons Attribution License, which permits unrestricted use, distribution, and reproduction in any medium, provided the original work is properly cited.

This article has been retracted by Hindawi following an investigation undertaken by the publisher [1]. This investigation has uncovered evidence of one or more of the following indicators of systematic manipulation of the publication process:

- (1) Discrepancies in scope
- (2) Discrepancies in the description of the research reported
- (3) Discrepancies between the availability of data and the research described
- (4) Inappropriate citations
- (5) Incoherent, meaningless and/or irrelevant content included in the article
- (6) Manipulated or compromised peer review

The presence of these indicators undermines our confidence in the integrity of the article's content and we cannot, therefore, vouch for its reliability. Please note that this notice is intended solely to alert readers that the content of this article is unreliable. We have not investigated whether authors were aware of or involved in the systematic manipulation of the publication process.

Wiley and Hindawi regrets that the usual quality checks did not identify these issues before publication and have since put additional measures in place to safeguard research integrity.

We wish to credit our own Research Integrity and Research Publishing teams and anonymous and named external researchers and research integrity experts for contributing to this investigation.

The corresponding author, as the representative of all authors, has been given the opportunity to register their agreement or disagreement to this retraction. We have kept a record of any response received.

### References

- [1] J. Gao, S. Xie, X. Zhang, H. Wang, W. Gao, and H. Zhou, "Study on the 2D Optimization Simulation of Complex Five-Hole Cutting Blasting under Different Lateral Pressure Coefficients," *Complexity*, vol. 2020, Article ID 4639518, 12 pages, 2020.

## Research Article

# Study on the 2D Optimization Simulation of Complex Five-Hole Cutting Blasting under Different Lateral Pressure Coefficients

Jing Gao,<sup>1</sup> Shizhen Xie,<sup>1</sup> Xiantang Zhang <sup>1,2</sup> Hongli Wang,<sup>2</sup> Wenle Gao,<sup>1</sup> and Hongmin Zhou<sup>1</sup>

<sup>1</sup>School of Civil Engineering and Architecture, Shandong University of Science and Technology, Qingdao 266590, China

<sup>2</sup>Shandong Provincial Key Laboratory of Civil Engineering Disaster Prevention and Mitigation, Shandong University of Science and Technology, Qingdao 266590, China

Correspondence should be addressed to Xiantang Zhang; zzxhtm@sdust.edu.cn

Received 4 April 2020; Accepted 12 May 2020; Published 10 June 2020

Guest Editor: Zhihan Lv

Copyright © 2020 Jing Gao et al. This is an open access article distributed under the Creative Commons Attribution License, which permits unrestricted use, distribution, and reproduction in any medium, provided the original work is properly cited.

With the decrease and depletion of shallow coal resources, the depth of mining is increasing. The mechanism of high crustal stress blasting is not clear, and the effect of crustal stress on blasting effect is obvious. The law of the differential detonation is similar without crustal stress. The crustal stress of rock masses increases linearly with the increase in excavation depth, and the influence of crustal stress on blasting effect is great. In order to study the rock-breaking process of complex differential blasting under deep high crustal stress, the instantaneous detonation of each model and the priority detonation of the central hole are numerically simulated. The evolution law of the blasting crack and the method of optimizing blasting effect by differential blasting and increasing the aperture of the priority detonation hole under high crustal stress are put forward. The authors proposed a study on the 2D optimization simulation of complex five-hole cutting blasting under different lateral pressure coefficients of 400 m and 800 m with software ANSYS/LS-DYNA and analyzed the evolution rules of blasting cracks and lateral pressure coefficients. The results show that setting delayed detonation and hole diameter and optimizing blasthole spacing can optimize the rock-breaking effect under high crustal stress and different lateral pressure coefficients.

## 1. Introduction

With the reduction and depletion of shallow coal resources, deep mining has become an inevitable trend. With the passage of time, the future will be mined towards deeper rock formations. In the current excavation process of the deep rock mass, the drilling and blasting method is still the main method of rock breaking. As the depth of the excavation increases, the influence of the initial crustal stress on the blasting effect becomes more and more important. According to the variation of vertical and horizontal stress with depth in various countries given by Brady and Brown, the vertical stress generally increases linearly with the increase of depth, and the variation law of horizontal stress is more complicated, which makes the blasting excavation of deep rock mass have great difficulties [1, 2]. At present, the research on deep rock mass mining is still in the initial stage,

the design of excavation parameters is still based on the design method of shallow rock mass blasting, and the influence of initial crustal stress is not considered enough, which makes the blasting effect poor, the excavation speed slow, the late support time long, and even have the rock burst and other major disasters. This makes it particularly important to study blasting rock breaking under initial crustal stress, and it is particularly urgent to study the design of blasting parameters and the rapid and safe excavation of rock mass stability under initial crustal stress.

In view of the rock-breaking mechanism of deep rock mass under initial crustal stress, scholars at home and abroad have carried out extensive research on physical experiment and numerical simulation. Based on the stress state equation of the rock mass in the cut area established by Schwarz alternating iteration method and elastic mechanics theory, two-dimensional numerical simulation of

straight cut blasting under different stress fields was carried out, and the maximum tensile stress was generated on the line connecting the hollow hole and the slot hole after the initial crustal stress field and the explosion stress field were combined by the rock mass [2]. The damaged model of rock blasting built on the basis of damaged mechanics analyzed the influence of different lateral pressure coefficients and buried depth on the crack growth rule [3]. The coupling model of Cowper–Symonds hardening model and tension and compression damaged model was embedded in LS-DYNA software for a two-dimensional numerical simulation. It was found that the central hole had an impact on rock damage [4]. Blasting parameter design method is suitable for deep high-stress rock roadway excavation by using numerical simulation and field test [5]. Wang et al. did numerical simulation by creep experimental data, obtained the creep equation of the surrounding rock in the deep soft rock roadway under high crustal stress, and established the quantitative creep relationship between time and stress [6]. He et al. summarized and analyzed the main differences of rock mass mechanical properties between deep mining and shallow mining through experiments [7]. The theoretical calculation model of the fragmentation size distribution containing the damage variable is proposed. Simulations and tests show that the action of the extrusion and collision between motive fragment blocks is a significant factor affecting the average fragmentation size regardless of the type of rock mass, especially for the rock mass with very bad quality [8]. The new model named MAGRM is a group recommendation model based on multiattention. It can well utilize multiattention-based deep neural network structures to achieve accurate group recommendation [9]. Based on LS-DYNA finite element program, NA finite element program, and optimization of cutting blasting in high-speed drivage process of an iron mine roadway, the authors carried out a study about numerical simulation and field test to the cutting blasting method with different blasting holes [10]. In order to eliminate the simplification of the interaction in data processing and improve the generated working efficiency, a method of redundant electrode determination based on the theory of variance is proposed [11]. Simulation of the complex rock-breaking mechanism under crustal stress included the prediction model of carbonation depth of slag high-performance concrete [12, 13]. Based on rock blasting theory, the authors used ANSYS/LS-DYNA to simulate the process of rock fragmentation of double-blasthole blasting with one empty hole at the center position [14]. The crack propagation in the rock under composite stress was studied by using digital image correlation technique [15]. The design and realization of the magnetic suspension controller are discussed, and a nonlinear mathematical model of the magnetic suspension system is built [16]. Based on the theory of the BP neural network and the engineering geological database as the research and development platform, this paper establishes the prediction of geotechnical parameters based on the analysis of the characteristics of geotechnical materials and the distribution of geotechnical sediments and geotechnical

parameters [17]. Local plane wave decomposition method considered from the perspective of inversion is employed to obtain higher-quality slant stack data, and the dynamic focused beam propagator is adopted to control the divergence of beams [18]. To reduce the impact of blasting vibration on the existing tunnel during the excavation of small-distance tunnel blasting, software was used to simulate the blasting vibration of the tunnel in different positions and forms [19].

Under the action of crustal stress, two-dimensional numerical simulation of complex five-hole blasting under different lateral pressure coefficients is carried out using ANSYS/LS-DYNA. Aiming at the differential detonation and increasing the diameter of the central blasthole under high crustal stress, the simulation study is provided for the blasting construction of deep rock mass.

## 2. Theoretical Analysis of Rock State with Different Confining Pressures and Lateral Pressure Coefficients

The drilling of the rock under the condition of initial crustal stress has changed the original stable state of the rock so that the rock around the blasthole produces an instant loosening zone. Since the blasthole is relatively small compared to the roadway, the concentrated stress value around the blasthole is smaller than the rock strength, the surrounding rock is in an elastoplastic state, and the surrounding rock is self-stabilizing. However, the stability of the loosening zone around the blasthole is less than that of the original rock. Similar to the loosening circle theory, in bidirectional confining pressure (side lateral pressure coefficient is equal to 1), vertical stress and horizontal stress are equal, the loosening zone is circular, the rock stability around the blasthole is evenly distributed, and the direction of rock crack propagation after explosion is randomly distributed, which is inhibited by the crustal stress. In the case of bidirectional unequal confining pressure (lateral pressure coefficient is not equal to 1), vertical stress and horizontal stress are not equal, the loosening zone is elliptic, and the long axis of the ellipse is perpendicular to the direction of the maximum crustal stress. Rock around the blasthole is affected by the initial stress field, and the explosion crack is restrained by the crustal stress and mainly expands to the side with large crustal stress. Figures 1–3, respectively, show the effect diagrams when the lateral pressure coefficient is 1, 0.2, and 4 under the initial vertical stress of 10 MPa. As can be seen from the figure, when the lateral pressure coefficient  $\lambda = 1$ , uniform stress concentrations are produced around the rock. When the lateral pressure coefficient  $\lambda = 0.2$  and 4, the tensile stress concentration is generated on the side with larger crustal stress. The maximum tensile stress is generated by the coupling of crustal stress and explosion stress under the action of constant pressure on both sides, this analysis analyzed the cause of the maximum tensile stress and the influence of different side pressures on the maximum tensile stress direction from the initial stress of the blasthole [2].

The initial stress state of the rock has an important effect on the blasting rock. Rock blasting under the initial stress

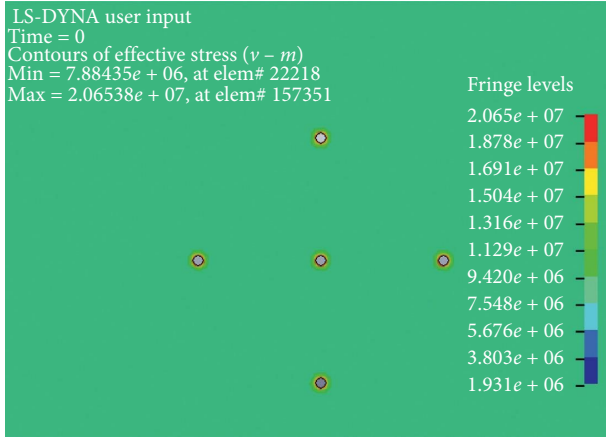


FIGURE 1: The effect diagram when the lateral pressure coefficient is 1.

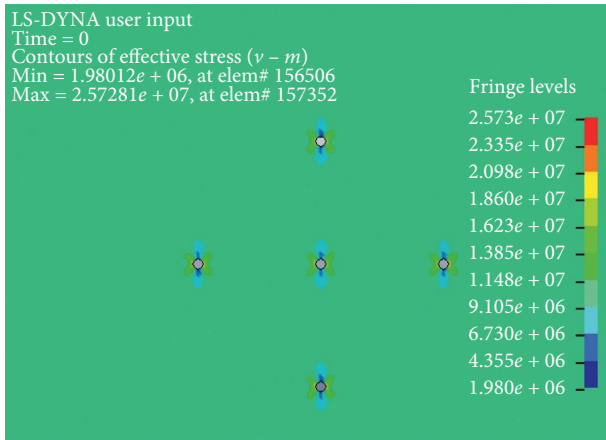


FIGURE 2: The effect diagram when the lateral pressure coefficient is 0.2.

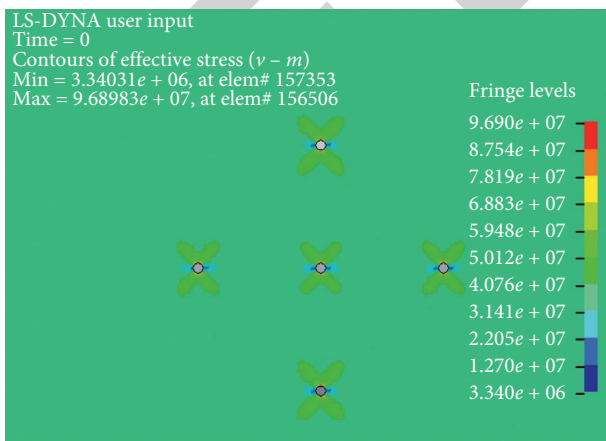


FIGURE 3: The effect diagram when the lateral pressure coefficient is 0.4.

condition is the effect of the coupling field formed by the coupling of the stress field redistributed in the rock around the blasthole and the explosive stress field after the explosion.

2.1. Calculation of the Initial Crustal Stress Field of the Rock. Radial effective stress  $\sigma_{r0}$ , tangential effective stress  $\sigma_{\theta0}$ , and shear stress of the rock  $\tau_{r\theta}$  around the blasthole under initial crustal stress can be calculated according to the elastic theory [20]:

$$\begin{cases} \sigma_{r0} = \frac{\sigma_H + \sigma_h}{2} \left(1 - \frac{R^2}{L^2}\right) + \frac{\sigma_H - \sigma_h}{2} \left(1 + \frac{3R^4}{L^4} - \frac{4R^4}{L^4}\right) \cos 2\theta, \\ \sigma_{\theta0} = \frac{\sigma_H + \sigma_h}{2} \left(1 + \frac{R^2}{L^2}\right) + \frac{\sigma_H - \sigma_h}{2} \left(1 + \frac{3R^4}{L^4}\right) \cos 2\theta, \\ \tau_{r\theta} = \frac{\sigma_H - \sigma_h}{2} \left(1 - \frac{3R^4}{L^4} + \frac{2R^4}{L^4}\right) \sin 2\theta, \end{cases} \quad (1)$$

where  $\sigma_H$  and  $\sigma_h$  are the maximum and the minimum horizontal crustal stress;  $\theta$  is the angle between the radial direction of the point around the hole and the direction of the maximum horizontal crustal stress;  $R$  is the radius of the blasthole; and  $L$  is the distance from the calculation point to the center of the blasthole.

2.2. Calculation of the Rock Stress under Explosive Load.

The stress state around the rock is further changed by the reflection and tension of the stress wave on the rock around the blasthole under the explosion stress [21]. The radial stress of an explosion at a certain point in the rock  $\sigma_{r1}$  and the tangential stress of an explosion at a certain point in the rock  $\sigma_{\theta1}$  can be calculated according to the attenuation formula of the stress wave [22]:

$$\begin{cases} \sigma_{r1} = p_0 \left(\frac{L}{R}\right)^{-\alpha}, \\ \sigma_{\theta1} = -\lambda_d \sigma_r, \end{cases} \quad (2)$$

where  $p_0$  is the initial pressure acting on the hole wall after the explosion of the explosive; the value of  $\alpha$ , stress wave attenuation coefficient, is  $2 - (\mu_d/1 - \mu_d)$ ;  $\mu_d$  is the dynamic Poisson ratio, and the relationship between it and the static Poisson ratio is  $\mu_d = 0.8\mu$ ; and  $\lambda_d$  is the dynamic lateral stress coefficient, and its value is  $\lambda_d = (\mu_d/1 - \mu_d)$ .

Therefore, the tangential stress after superposition is  $\sigma_r = \sigma_{r0} + \sigma_{r1}$ . That is, when the tangential stress in the rock is greater than the ultimate tensile strength of the rock under the combined action of the initial stress and the explosion stress, the rock will produce cracks, and then failure occurs.

### 3. Establishment of a Numerical Model for Rock Blasting

3.1. Rock Constitutive Model and Material Parameters. In order to observe the change of the rock damaged vertically and horizontally under the initial crustal stress field, the theoretical model of complex five-hole cutting blasting is selected under the condition of RHT rock constitutive, the fixed constraint is applied to the bottom of the model, the surrounding compressive stress is applied in the other

three directions, and the initial crustal stress field is simulated by using the implicit-display order of DYNA [23]. Because the law mainly analyzes and summarizes the damage degree of the rock, it does not involve the formation process of the groove cavity, and it directly simulates the damage evolution process of rock profile with a thickness of 0.01 m. When the computer carries out the numerical simulation, the mesh quality affects the accuracy of the numerical simulation, and the size of the mesh division and the number of the quantity affect the accuracy of the simulation. The model size is  $5\text{ m} \times 4\text{ m} \times 0.01\text{ m}$ , wherein 5 blastholes with a radius of 20 mm are arranged, and the blasthole spacing is 0.5 m. Because the aperture size of the blasthole is small relative to the model size and the interface size does not change vertically with the model, the simulation can be reduced to a plane strain problem calculated by a single layer mesh, and the model is shown in Figure 4.

The explosive material model adopts \*MAT\_HIGH\_EXPLOSIVE\_BURN, using the JWL state equation, and the specific explosive parameters are shown in Table 1 [24]. Rock mechanics parameters are shown in Table 2 [25].

The JWL equation of the state defines that the pressure is

$$p = A \left( 1 - \frac{w}{R_1 V} \right) e^{-R_1 V} + B \left( 1 - \frac{w}{R_2 V} \right) e^{-R_2 V} + \frac{wE}{V}, \quad (3)$$

where  $p$  is the pressure of the detonation product;  $V$  is the relative volume of the detonation product;  $E$  is the initial internal energy density of the detonation product; and  $A$ ,  $B$ ,  $R_1$ ,  $R_2$ , and  $w$  are material parameters.

The material for the cell is \*MAT\_NULL. Defining the mass, the modulus of elasticity, Poisson's ratio, and so on, to define the material. The air material model uses MAT\_NULL air material model, its state equation is defined by the keyword EOS\_LINEAR\_POLYNOMIAL, and the state equation is as follows:

$$p = C_0 + C_1\mu + C_2\mu^2 + C_3\mu^3 + (C_4 + C_5\mu + C_6\mu^2)E, \quad (4)$$

where  $C_i$  is the equation parameter and  $E$  is the unit initial internal energy of relative volume  $\mu = (1/V) - 1$ ,  $V$  is the relative volume. Parameters of air material and state equations are shown in Table 3.

### 3.2. Loading Scheme of Crustal Stress with Different Lateral Pressure Coefficients in Blasting Damage

- (1) When the lateral pressure coefficient is  $\lambda = 1$ , model A:  $\sigma_z$  takes 10 MPa and corresponds to 400 m buried depth; model B:  $\sigma_z$  takes 20 MPa and corresponds to 800 m buried depth
- (2) When the lateral pressure coefficient is  $\lambda = 0.2$ , model C:  $\sigma_z$  takes 10 MPa,  $\sigma_x$  to 2 MPa, and model D:  $\sigma_z$  takes 20 MPa,  $\sigma_x$  to 4 MPa
- (3) When the lateral pressure coefficient is  $\lambda = 4$ , model E:  $\sigma_z$  takes 10 MPa,  $\sigma_x$  to 40 MPa, and model F:  $\sigma_z$  takes 20 MPa,  $\sigma_x$  to 80 MPa

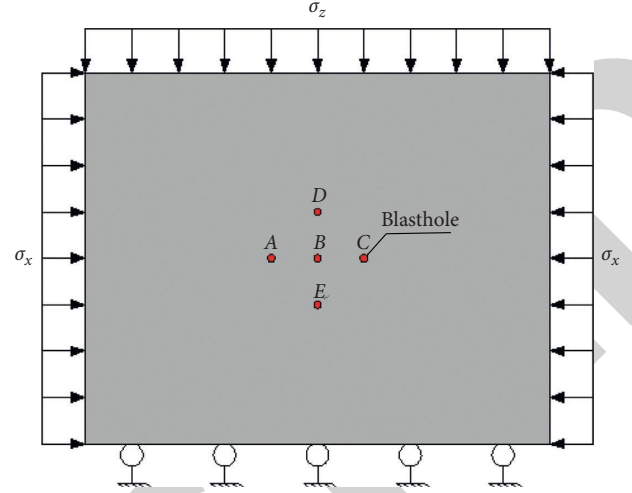


FIGURE 4: Numerical model under a single layer mesh.

TABLE 1: Establishment of the numerical model for blasting damage.

Density	Blast speed	CJ pressure	JWL state equation parameters					
			A	B	$R_1$	$R_2$	$\omega$	E
$\text{kg}\cdot\text{m}^{-3}$	$\text{m}\cdot\text{s}^{-1}$	GPa	(GPa)	(GPa)				(GPa)
1,300	6,000	3.240	220	0.2	4.5	1.1	0.35	4.2

## 4. Numerical Simulation Results and Analysis

In order to study the rock-breaking process of differential blasting under deep high crustal stress, the instantaneous detonation of each model and the prior detonation of the central hole are numerically simulated. The differential blasting initiation model sets the central hole to detonate first, and the remaining holes are set 50  $\mu\text{s}$  time delay and compared under different lateral pressure coefficients; the cloud map is output and analyzed after the computing cluster.

**4.1. Rock Damage Evolution Process with Lateral Pressure Coefficient Equal to 1.** Because the lateral pressure coefficient is equal to 1, the pressure around the hole is evenly distributed; in the early stage of the explosion, the explosion shock wave first acts on the rock mass around the hole so that the rock mass around the blasthole first produces damage. Before 50  $\mu\text{s}$ , the range of the rock damage around the blasthole under the same crustal stress model was similar, the explosion crushing area was basically molded, and the stress wave was not enough to produce direct damage to the rock mass while resisting the crustal stress and began to continue along the damaged area that had been formed. The damage range of the rock is comparable under 10 MPa and 20 MPa crustal stress, and there is no great difference. After 50  $\mu\text{s}$ , with the gradual attenuation of the stress wave, the inhibition of the crustal stress on the blasting effect began to show the following: due to the gradual attenuation of the stress wave, the influence of crustal stress on blasting effect is more and more in the later stage of

TABLE 2: Numerical model rock-specific parameters.

Parameter	Value	Parameter	Value
Mass density RO ( $\text{kg/m}^3$ )	2,660	Porosity exponent NP	3.0
Initial porosity ALPHA	0	Reference compressive strain rate EOC	$3.E-5$
Crush pressure PEL (MPa)	125	Reference tensile strain rate EOT	$3.E-6$
Compaction pressure PCO (GPa)	6.0	Break compressive strain rate EC	$3.E+25$
Hugoniot polynomial coefficient A1 (GPa)	25.7	Break tensile strain rate ET	$3.E+25$
Hugoniot polynomial coefficient A2 (GPa)	37.84	Compressive strain rate dependence exponent BETAC	0.026
Hugoniot polynomial coefficient A3 (GPa)	21.29	Tensile strain rate dependence exponent BETAT	0.007
Parameter for polynomial EOS B0	1.22	Volumetric plastic strain fraction in tension PTF	0.001
Parameter for polynomial EOS B1	1.22	Compressive yield surface parameter GC*	0.53
Parameter for polynomial EOS T1 (GPa)	25.7	Tensile yield surface parameter GT*	0.7
Parameter for polynomial EOS T2	0.0	Erosion plastic strain EPSF	2.0
Elastic shear modulus SHEAR (GPa)	21.9	Shear modulus reduction factor XI	0.5
Compressive strength FC (MPa)	167.8	Damage parameter D1	0.04
Relative tensile strength FT*	0.04	Damage parameter D2	1.0
Relative shear strength FS*	0.21	Minimum damaged residual strain EPM	0.015
Failure surface parameter A	2.44	Residual surface parameter AF	0.25
Failure surface parameter N	0.76	Residual surface parameter AN	0.62
Lode angle dependence factor Q0	0.68	Gruneisen gamma GAMMA	0.0
Lode angle dependence factor B	0.05		

TABLE 3: Parameters of air material and state equations.

Density ( $\text{g}\cdot\text{cm}^3$ )	$C_0$	$C_1$	$C_2$	$C_3$	$C_4$	$C_5$	$C_6$	$E$ (GPa)
$1.29E-5$	0	0	0	0	0.4	0.4	0	0.025

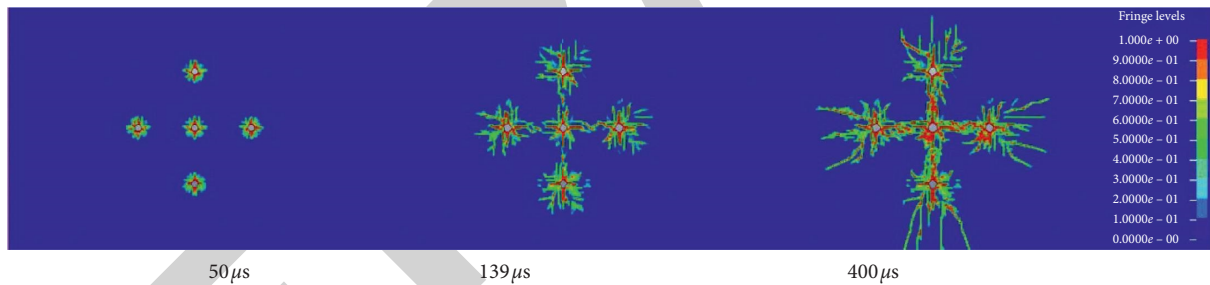


FIGURE 5: Damage evolution process diagram of model A.

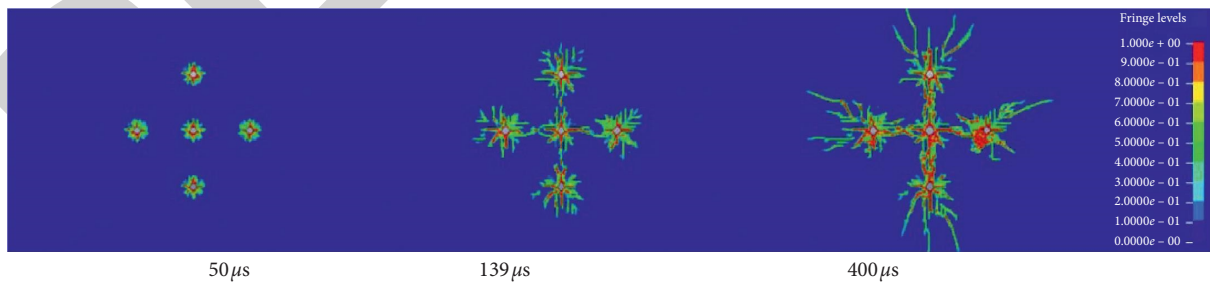


FIGURE 6: Damage evolution process diagram of model B.

explosion, and it can be seen from the final damage cloud map that the damage range and damaged degree of model A are obviously higher than those of model B; the greater the initial crustal stress, the greater the attenuation speed of the

wave. Figures 5 and 6, respectively, show the damage evolution process of models A and B.

Because the lateral pressure coefficient is equal to 1, the evolution of differential blasting damage is also inhibited by

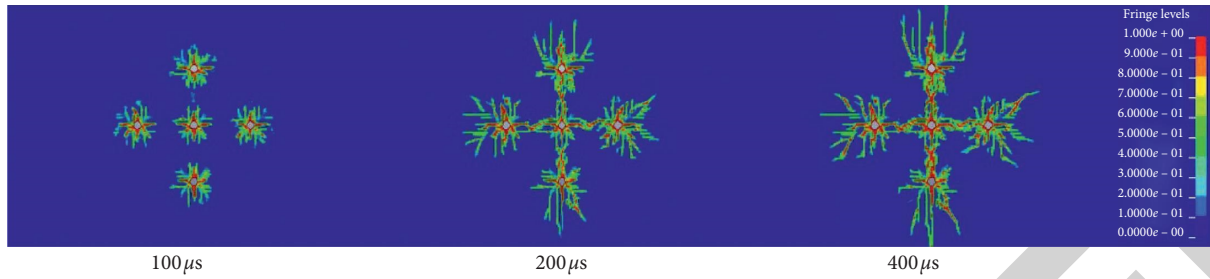


FIGURE 7: Damage evolution process diagram of model C.

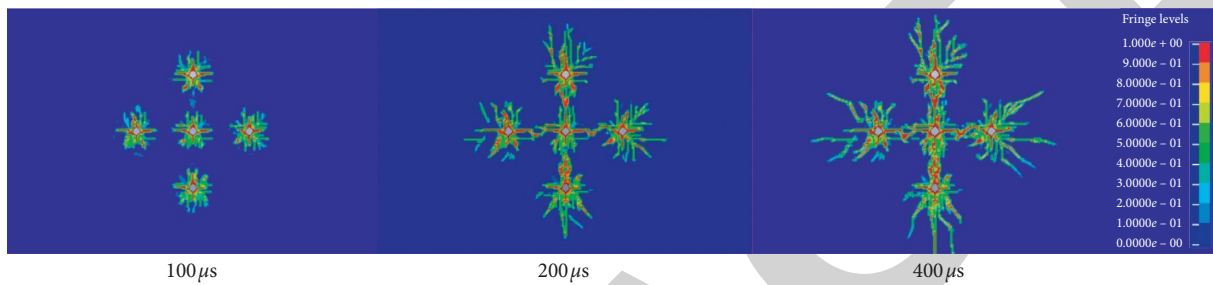


FIGURE 8: Damage evolution process diagram of model D.

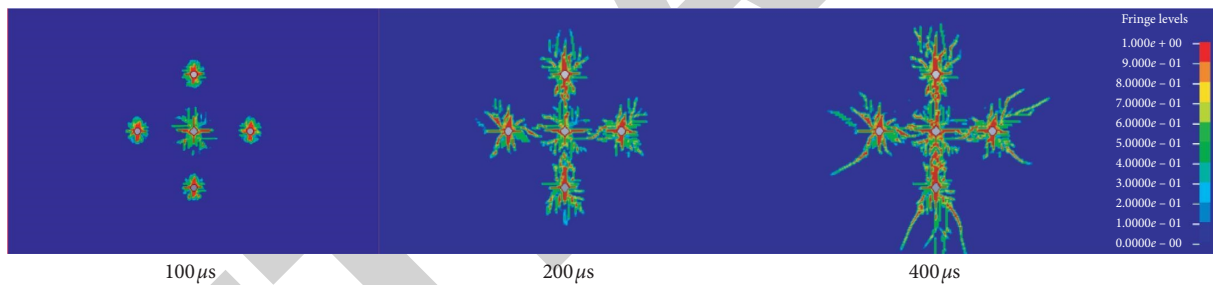


FIGURE 9: Differential initiation damage evolution process diagram of model D.

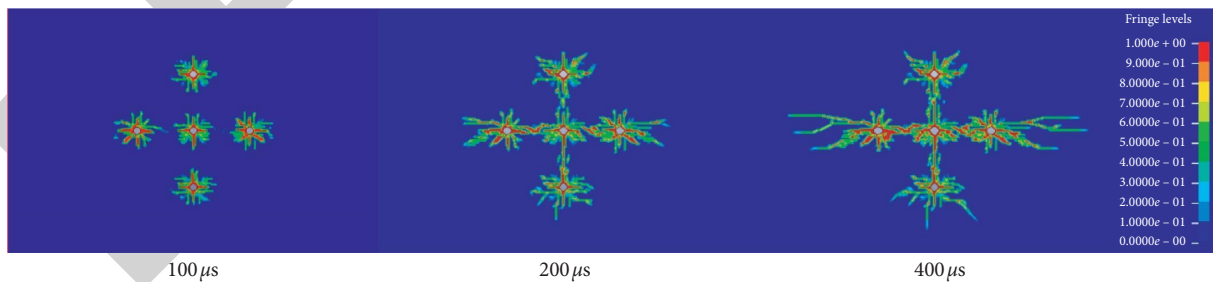
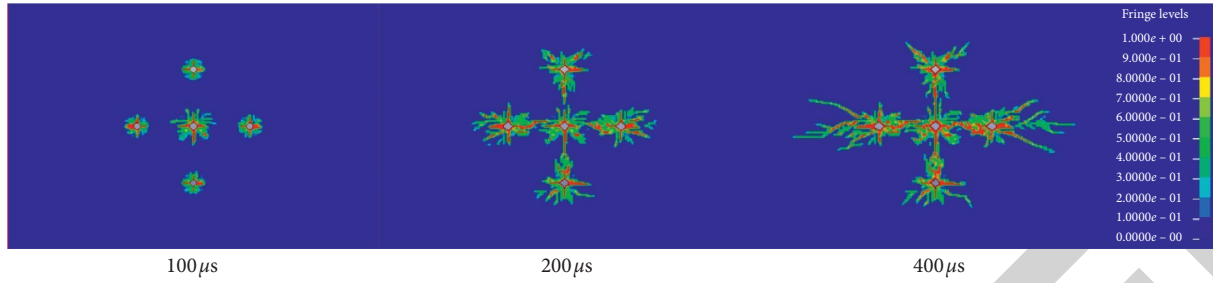
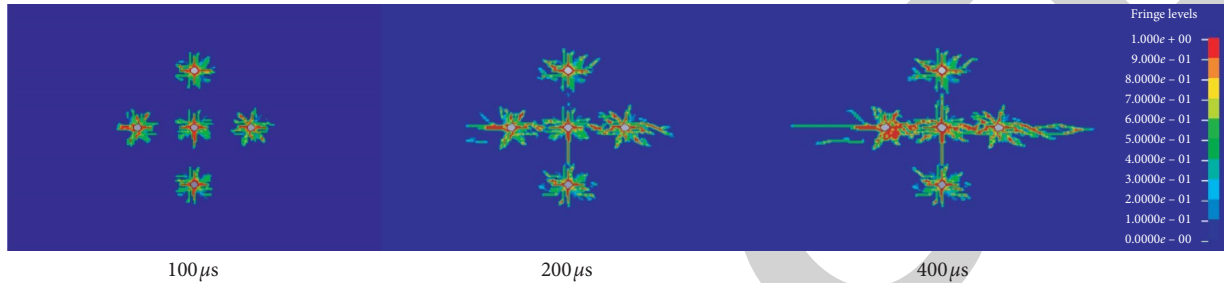
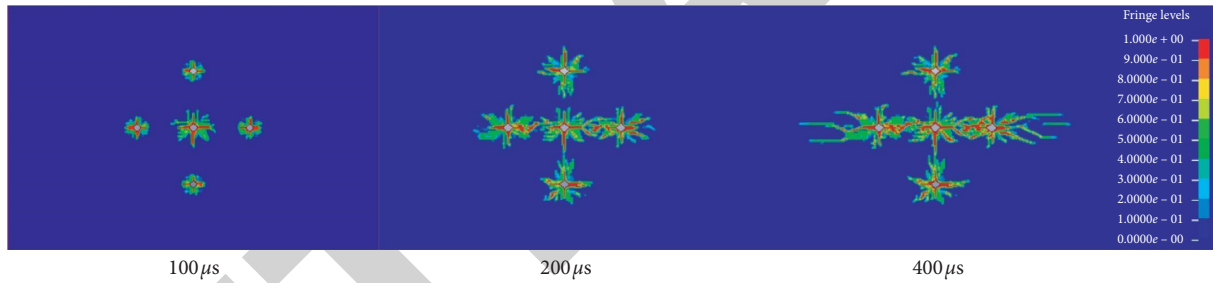
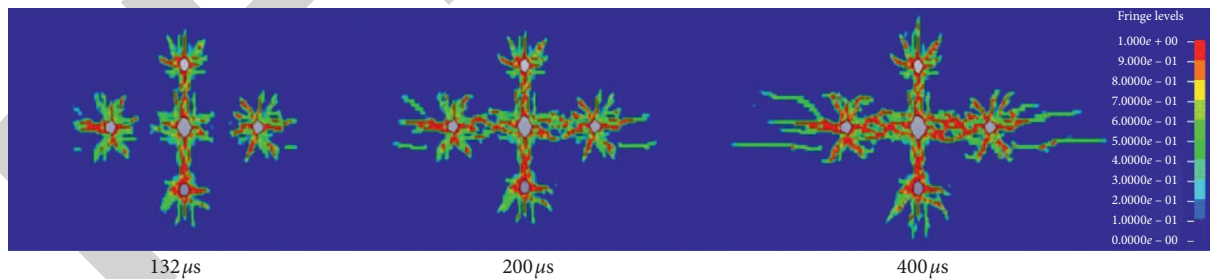


FIGURE 10: Instantaneous detonation damage evolution process cloud map of model E.

the crustal stress, but its evolution law is similar to that of noncrustal stress, so it is no longer described.

*4.2. Rock Damage Evolution Process with Lateral Pressure Coefficient Equal to 0.2.* By analyzing the damage evolution process with a lateral pressure coefficient of 0.2, it can be found that when the lateral pressure coefficient is 0.2, the

initial crustal stress around the hole is smaller when the bidirectional crustal stress is equal, so the inhibition of the initial crustal stress on the rock damage evolution is relatively small at this time. From the damage cloud diagram, it can be seen that because the crustal stress in the vertical direction is greater than the crustal stress in the horizontal direction, the rock damage mainly develops in the vertical direction, the damage range of the hole connection in the

FIGURE 11: Differential initiation damage evolution process diagram of model *E*.FIGURE 12: Instantaneous detonation damage evolution process cloud map of model *F*.FIGURE 13: Differential initiation damage evolution process diagram of model *F*.FIGURE 14: Instantaneous detonation damage evolution process cloud map of model *G*.

vertical direction is larger than the horizontal direction, and the guiding effect of the crustal stress on the crack propagation begins to show. Compared with models *C* and *D*, although the side pressure coefficient is the same, the gap between  $\sigma_z$  and  $\sigma_x$  of model *D* is larger, the guidance effect of model *D* on damage evolution is more obvious, and the damage evolution speed and damage range in the vertical direction are larger than those of model *C*; the gap between  $\sigma_z$  and  $\sigma_x$  in model *C* is smaller, the damage evolution

process in the horizontal and vertical direction is slightly different, but the damage range in the direction of the final hole connection is not much different. It can be seen that the guiding effect and inhibition of crustal stress on damage evolution are not linear. The damage evolution process for models *C* and *D* is shown in Figures 7 and 8.

Because the blasting effect of model *D* in the horizontal direction is not ideal, the central hole is set to detonate first, and the other holes are set to  $50 \mu\text{s}$  time-delay detonation.

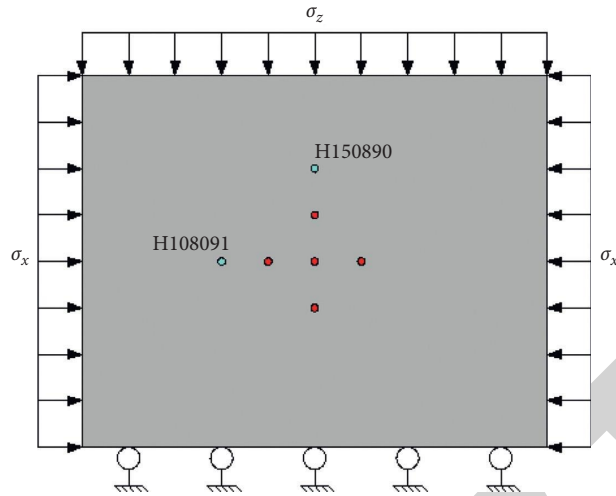
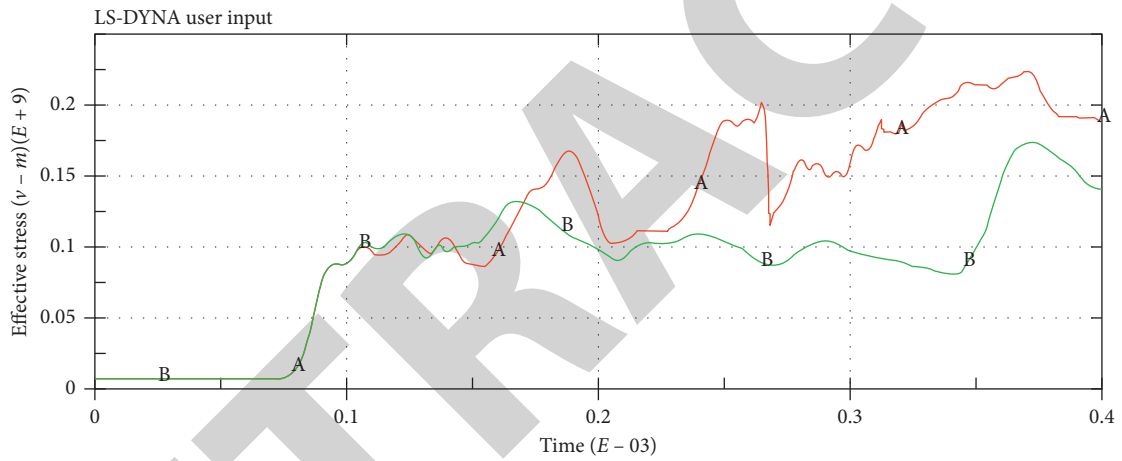
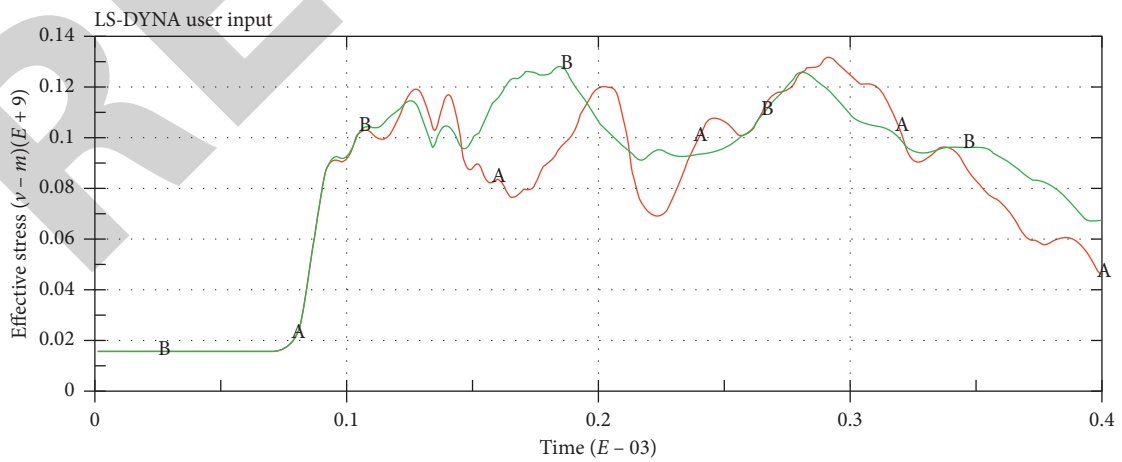


FIGURE 15: Selection diagram of observation points.



Element no.  
A 150890  
B 108091

(a)



Element no.  
A 150890  
B 108091

(b)

FIGURE 16: Equivalent stress diagram of observation point. (a) Two-way confining pressure is 10 MPa. (b) Two-way confining pressure is 20 MPa.

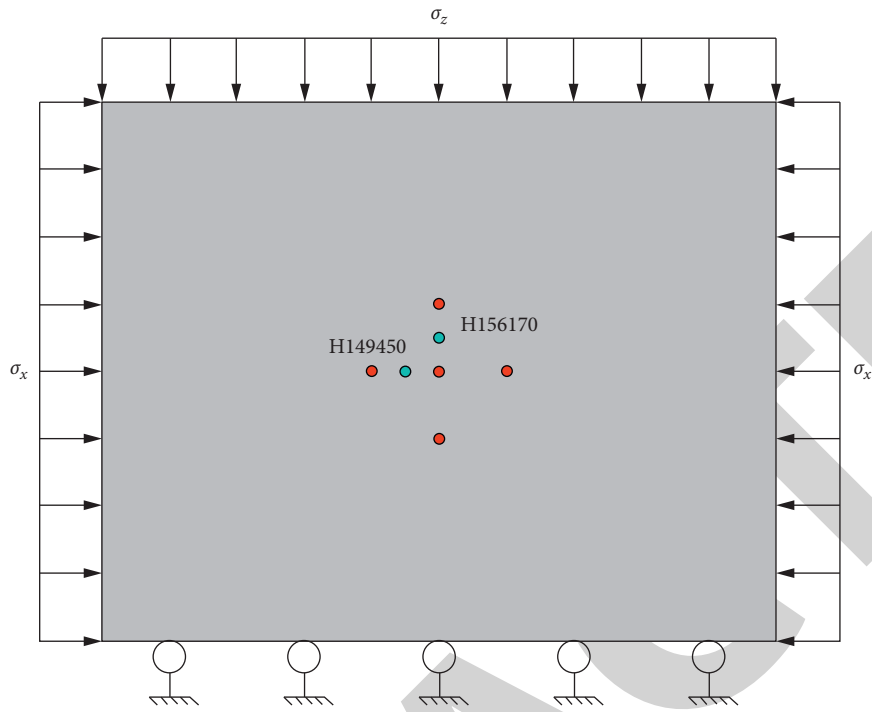
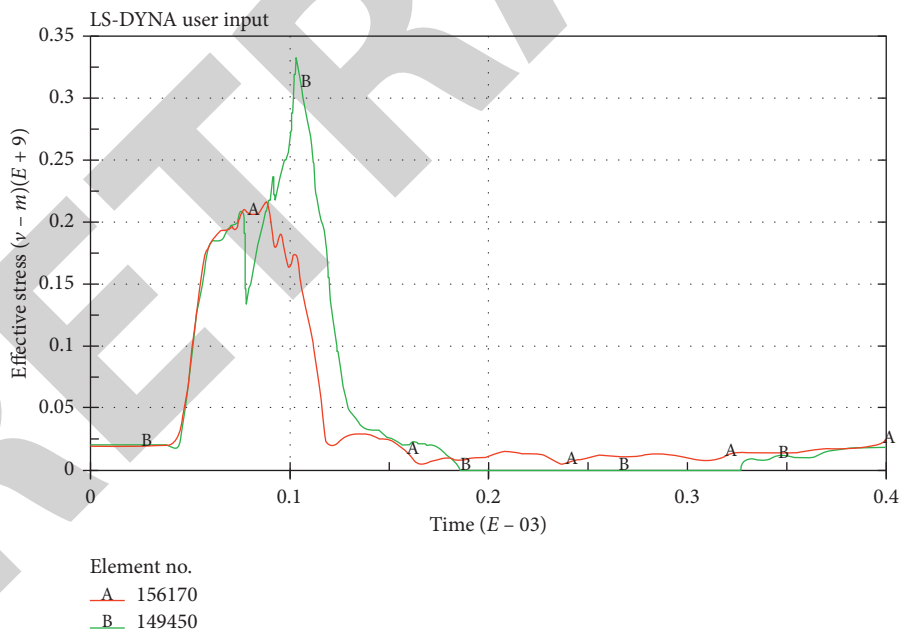
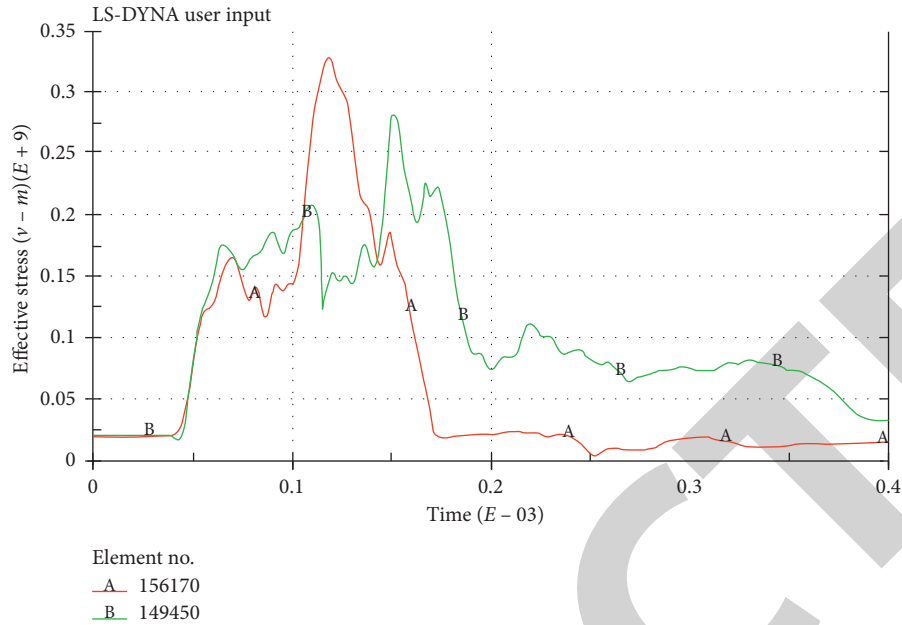


FIGURE 17: Model *D* selects unit location.



(a)

FIGURE 18: Continued.



(b)

FIGURE 18: Comparison of the effective stress time-history curve of the selected element in model *D*. (a) Model *D* time-history curve of effective stress of multichoice element differential blasting. (b) Model *D* time-history curve of effective stress of multichoice element instantaneous blasting.

The damage evolution diagram of model *D* is shown in Figure 9. Compared with the instantaneous detonation, the damage range of the rock is obviously larger than that of instantaneous detonation, the guiding effect of high crustal stress on damage evolution is weakened, the range of horizontal damage is obviously increased, the damage zone on the outside of the vertical hole is shortened, and it is beneficial to the measures such as late support.

**4.3. Rock Damage Evolution Process with Lateral Pressure Coefficient Equal to 4.** With the increase of crustal stress, the inhibitory effect on rock damage evolution increases gradually, while the damaged area is further concentrated in the maximum crustal stress direction, the damage evolution speed in the direction of the maximum crustal stress is accelerated, the region of damage on the outside of the hole is increased, and rock blasting under the initial crustal stress is more difficult. The optimization effect of differential detonation on blasting effect is weakened, which mainly promotes rock damage of the intersection position of the stress wave, and the coupling field between stress wave and crustal stress beyond the limit tensile strength of the rock is further reduced and concentrated. The instantaneous and differential damage evolution diagram of models *E* and *F* with lateral pressure coefficient equal to 4 is, respectively, shown in Figures 10–13.

In model *F*, due to the large difference between  $\sigma_z$  and  $\sigma_x$ , the damage area in the vertical direction is not penetrated. At this time, in the case of differential blasting, it can be considered to increase the diameter of the central hole and shorten the hole spacing on the side with smaller crustal

stress. The model increases the diameter of the central hole to 30 mm, and the blasthole spacing decreases to 0.3 m for numerical simulation, defined as model *G*. The simulation results show that the vertical direction damage is already running through at 132  $\mu$ s, and the damage degree and damage area are still increasing, the final hole is completely running through, increasing the utilization rate of the hole, the difference of damage range in two directions decreases, and there will be no situation similar to that of model *F* blasting. The damage evolution process for model *G* is shown in Figure 14.

**4.4. Simulation Analysis of Five-Hole Cutting Blasting Results.** From the above model and simulation improvement, it can be seen that differential blasting plays a certain role in optimizing the blasting effect under the action of crustal stress, and with the increase of crustal stress, the optimization effect of differential blasting decreases gradually so that reducing the hole spacing in the smaller direction of crustal stress can achieve the optimization effect, and further optimization can increase the diameter of the central hole; in order to meet the blasting demand under the high crustal stress, the utilization rate of the blasthole is improved.

The attenuation law of the stress wave under crustal stress is observed at two observation points H150890 and H108091 in the same position when bidirectional compressive stress is 10 MPa and 20 MPa, respectively, and the selection position is shown in Figure 15.

From the equivalent stress-time curve of the two models, it can be seen that the time for the observation point to reach the first stress peak is similar, around 127  $\mu$ s, which is

because the observation point is close to the hole spacing, the force on the stress wave is not obvious, and the effective stress is around 115 MPa; when the observation point reaches its second peak, at this point, the stress wave begins to overlay, the crustal stress corresponds to the role of the wave which began to produce differences; for the observation points H150890 and H108091 in the confining pressure of 10 MPa, the peak time and size are (189  $\mu$ s, 168 MPa) and (166  $\mu$ s, 132 MPa), and when the confining pressure is 20 MPa, the peak time and size are (205  $\mu$ s, 120 MPa) and (185  $\mu$ s, 126 MPa); combined with the peak data of Figure 16 [26], it can be seen that, with the increase of crustal stress, the influence on the propagation of the stress wave increases, which is reflected in the increase of stress wave velocity and stress size attenuation velocity.

In order to study the impact of differential blasting on rock damage under different lateral pressures, the time-history curves of effective stress of differential blasting and instantaneous blasting in model *D* were selected for comparative analysis. The selected unit is shown in Figure 17.

In Figure 18, the effective stress of model *D* decays rapidly after reaching the peak and decays to the initial crustal stress value at around 112  $\mu$ s, while the differential blasting has experienced stress wave superposition for many times, and the effect time is longer and decays to the effective stress value at around 160  $\mu$ s. It can be seen that the action time of differential blasting is long, which can promote the rock damage. In addition, its peak stress is smaller than that of instantaneous blasting, and the resulting vibration is smaller, which is conducive to the stability of the surrounding rock mass under high crustal stress.

## 5. Conclusions

Using finite element analysis software ANSYS/LS-DYNA, the rock damage of complex five-hole cutting blasting under different lateral pressure coefficients is numerically simulated, and two-dimensional simulation can divide more meshes than three-dimensional simulation at the same time, which can improve the accuracy of simulation when simulating complex blasting. Rock blasting under high crustal stress can be regarded as the damage caused by the coupling position of the rock in the explosion field and the crustal stress field, which is greater than the ultimate tensile strength of the rock.

Under the bidirectional pressure, the crack propagation is inhibited with the increase of crustal stress field, and the evolution law of differential blasting damage is similar to that of noncrustal stress field, which is inhibited by the initial crustal stress field. In the two-way unequal pressure, the direction of damage evolution tends to be on the side of large crustal stress field, and the guiding effect and inhibition of crustal stress field on damage evolution are nonlinear; the priority detonation of the central hole can optimize the blasting effect on the smaller side of the crustal stress field and shorten the damage length of the larger side of the crustal stress field, which decreases with the increase of the crustal stress field; at this time, we can consider increasing the diameter of the priority detonation hole under the

condition of differential blasting. At the same time, shortening the hole spacing on the smaller side of the crustal stress field can further improve the blasting effect. The stress wave velocity and the effective stress attenuation velocity increase with the increase of the crustal stress field.

## Data Availability

The data used to support the findings of this study are available from the corresponding author upon request.

## Conflicts of Interest

The authors declare no conflicts of interest.

## Acknowledgments

This study was supported by the National Natural Science Foundation of China (51874189 and 51709161), the Shandong Provincial Natural Science Foundation of China (ZR2017MEE043), the Visiting Scholar Fund of Shandong University of Science and Technology, and the Project of Shandong University of Science and Technology Graduate Innovation Fund (SDKDYC190241 and SDKDYC190242). The financial supports are gratefully acknowledged.

## References

- [1] E. T. Brown and E. Hoek, "Trends in relationships between measured in-situ stresses and depth," *International Journal of Rock Mechanics and Mining Sciences & Geomechanics Abstracts*, vol. 15, no. 4, pp. 211–215, 1978.
- [2] Q. T. Li, W. L. Huang, and Z. Y. Wu, "Theoretical study and numerical simulation on rock failure process in cutting by parallel hole under different crustal stress conditions," *Journal of Safety Science and Technology*, vol. 12, no. 11, pp. 57–62, 2016, in Chinese.
- [3] Y. Bai, W. C. Zhu, and C. H. Wei, "Numerical simulation on two-hole blasting under different in-situ stress conditions," *Rock and Soil Mechanics*, vol. 34, no. S1, pp. 466–471, 2013, in Chinese.
- [4] L. Xie, W. Lu, Q. Jiang, and Q. Zhang, "Damaged evolution mechanism of deep rock mass in process of cut blasting," *Journal of Central South University Science and Technology*, vol. 48, no. 5, pp. 1252–1260, 2016, in Chinese.
- [5] H. J. Wang, R. S. Yang, and Q. Li, "Analysis of blasting mechanism for deep rock tunneling and blasting parameters design," *Journal of China Coal Society*, vol. 4, pp. 373–376, 2007, in Chinese.
- [6] Y. Y. Wang, J. Wei, and J. Qi, "Study on prediction for nonlinear creep deformation of deep rocks," *Journal of China Coal Society*, vol. 4, pp. 409–413, 2005, in Chinese.
- [7] M. C. He, H. P. Xie, and S. P. Peng, "Research on rock mass mechanics in deep mining," *Chinese Journal of Rock Mechanics and Engineering*, vol. 16, pp. 2803–2813, 2005, in Chinese.
- [8] X. T. Zhang and S. H. Chen, "Study on blast fragmentation for jointed and fractured rock mass considering collision," *Chinese Journal of Rock Mechanics and Engineering*, vol. 21, no. 8, pp. 1141–1146, 2002, in Chinese.
- [9] Z. Huang, X. Xu, H. Zhu, and M. Zhou, "An efficient group recommendation model with multiattention-based neural

- networks,” *IEEE Transactions on Neural Networks and Learning Systems*, pp. 1–14, 2020.
- [10] X. T. Zhang and Y. G. Ji, “Comparative analysis on blasting effect of different cutting blasting for the sandstone tunnel drivage in iron mine,” *Journal of the Balkan Tribological Association*, vol. 22, no. 1A, pp. 1014–1029, 2016.
- [11] Y. Sun, C. Xu, G. F. Li et al., “Intelligent human computer interaction based on non redundant EMG signal,” *Alexandria Engineering Journal*, 2020.
- [12] X. T. Zhang, Z. X. Li, and Q. Ma, “Study on the correlation between shpc pore structure and air permeability,” *Tehnicki Vjesnik-Technical Gazette*, vol. 24, no. 5, pp. 1425–1430, 2017.
- [13] X. Zhang, X. Zhou, H. Zhou, K. Gao, and Z. Wang, “Studies on forecasting of carbonation depth of slag high performance concrete considering gas permeability,” *Applied Clay Science*, vol. 79, pp. 36–40, 2013.
- [14] H. Li, X. Zhang, D. Li, L. Wu, W. Gao, and H. Zhou, “Numerical simulation of the effect of empty hole between adjacent blast holes in the perforation process of blasting,” *Journal of Intelligent & Fuzzy Systems*, vol. 37, no. 3, pp. 3137–3148, 2019.
- [15] Y. W. Lv and C. P. Sun, “Experimental study on damage evolution and crack propagation characteristics of sandstone under combined stress state,” *Journal of Shandong University of Science and Technology (Natural Science)*, vol. 39, no. 1, pp. 37–45, 2020, in Chinese.
- [16] Y. Sun, J. Xu, H. Qiang, and G. Lin, “Adaptive neural-fuzzy robust position control scheme for Maglev train systems with experimental verification,” *IEEE Transactions on Industrial Electronics*, vol. 66, no. 11, pp. 8589–8599, 2019.
- [17] K. Cui and X. Jing, “Research on prediction model of geotechnical parameters based on BP neural network,” *Neural Computing and Applications*, vol. 31, no. 12, 2019.
- [18] H. Sun, C. Gao, Z. Zhang, X. Liao, X. Wang, and J. Yang, “High-resolution anisotropic prestack Kirchhoff dynamic focused beam migration,” *IEEE Sensors Journal*, p. 1, 2019.
- [19] Z. Sun, S. Z. Xie, and X. T. Zhang, “Vibration reduction effect of damping holes in blasting excavation of tunnels with small spacing,” *Journal of Shandong University of Science and Technology (Natural Science)*, vol. 38, no. 1, pp. 25–31+39, 2019, in Chinese.
- [20] C. R. Li, L. J. Kang, and Q. X. Qi, “Probe into relationship between zonal fracturing and rock burst in deep tunnel,” *Journal of China Coal Society*, vol. 35, no. 2, pp. 185–189, 2016, in Chinese.
- [21] Y. N. He, L. J. Han, and P. Shao, “Some problems of rock mechanics for roadways stability in depth,” *Journal of China University of Mining & Technology*, vol. 3, pp. 288–295, 2006, in Chinese.
- [22] L. Hu, Y. J. Wang, and G. F. Ren, “Experimental study on the best pattern of blasthole of shale,” *Blasting*, vol. 32, no. 4, pp. 44–48, 2015, in Chinese.
- [23] Y. S. Lou and Y. Q. Jin, *Rock Mechanics and Petroleum Engineering*, Petroleum Industry Press, Beijing, China, 2006, in Chinese.
- [24] X. Huang, H. N. Ruan, and X. W. Wang, “Stability analysis and control of deep soft rock roadway under different lateral pressure coefficients,” *China Coal*, vol. 44, no. 7, pp. 59–63+87, 2018, in Chinese.
- [25] L. X. Xie, W. B. Lu, Q. B. Zhang, Q. H. Jiang, M. Chen, and J. Zhao, “Analysis of damage mechanisms and optimization of cut blasting design under high in-situ stresses,” *Tunnelling and Underground Space Technology*, vol. 66, pp. 19–33, 2017, in Chinese.
- [26] W. Wei, X. Xia, and W. Marcin, “Multi-sink distributed power control algorithm for Cyber-physical-systems in coal mine tunnels,” *Computer Networks*, vol. 161, pp. 201–219, 2019.